




Regulation of Photosynthetic Carbohydrate Metabolism by a Raf-Like Kinase in the Liverwort *Marchantia polymorpha*

Eri Koide¹, Noriyuki Suetsugu ¹, Megumi Iwano¹, Eiji Gotoh², Yuko Nomura³, Sara Christina Stolze⁴, Hirofumi Nakagami^{3,4}, Takayuki Kohchi ¹ and Ryuichi Nishihama ^{1,*}

¹Graduate School of Biostudies, Kyoto University, Kyoto, 606-8502 Japan

²Faculty of Agriculture, Kyushu University, Fukuoka, 812-8581 Japan

³Plant Proteomics Research Unit, RIKEN CSRS, Yokohama, 230-0045 Japan

⁴Protein Mass Spectrometry Group, Max Planck Institute for Plant Breeding Research, Cologne 50829, Germany

*Corresponding author: E-mail, nishihama@lif.kyoto-u.ac.jp; Fax, +81-75-753-6127.

(Received November 1, 2019; Accepted December 12, 2019)

To optimize growth and development, plants monitor photosynthetic activities and appropriately regulate various cellular processes. However, signaling mechanisms that coordinate plant growth with photosynthesis remain poorly understood. To identify factors that are involved in signaling related to photosynthetic stimuli, we performed a phosphoproteomic analysis with *Marchantia polymorpha*, an extant bryophyte species in the basal lineage of land plants. Among proteins whose phosphorylation status changed differentially between dark-treated plants and those after light irradiation but failed to do so in the presence of a photosynthesis inhibitor, we identified a B4-group Raf-like kinase, named PHOTOSYNTHESIS-RELATED RAF (MpPRAF). Biochemical analyses confirmed photosynthesis-activity-dependent changes in the phosphorylation status of MpPRAF. Mutations in the MpPRAF gene resulted in growth retardation. Measurement of carbohydrates demonstrated both hyper-accumulation of starch and reduction of sucrose in *Mppraf* mutants. Neither inhibition of starch synthesis nor exogenous supply of sucrose alleviated the growth defect, suggesting serious impairment of *Mppraf* mutants in both the synthesis of sucrose and the repression of its catabolism. As a result of the compromised photosynthate metabolism, photosynthetic electron transport was downregulated in *Mppraf* mutants. A mutated MpPRAF with a common amino acid substitution for inactivating kinase activity was unable to rescue the *Mppraf* mutant defects. Our results provide evidence that MpPRAF is a photosynthesis signaling kinase that regulates sucrose metabolism.

Keywords: *Marchantia polymorpha* • Phosphoproteomics • Photosynthesis signaling • Raf-like protein kinase • Starch • Sucrose.

Accession numbers: The nucleotide sequence reported in this article has been submitted to DDBJ under accession number LC505674. The proteomics data generated in this study have

been submitted to ProteomeXchange and jPOST under accession numbers PXD015796 and JPST000685, respectively.

Introduction

To achieve optimal growth, plants must coordinate diverse cellular processes with photosynthesis activity. For instance, ongoing photosynthesis makes stomatal opening much more efficient (Suetsugu et al. 2014) and functional chloroplasts are essential for both stomatal opening and closure (Negi et al. 2018). Photosynthesis-derived sugars were shown to activate plasma membrane H⁺-ATPase (Okumura et al. 2012, Okumura et al. 2016), which is involved in various processes, including stomatal opening, cell expansion and intracellular pH homeostasis (Duby and Boutry 2009). Furthermore, photosynthetic sugars are known to activate axillary meristems (Mason et al. 2014) and to promote root growth by driving the TARGET OF RAPAMYCIN (TOR) signaling pathway (Kircher and Schopfer 2012, Xiong et al. 2013). Photosynthesis also generates retrograde signals. The redox status of the plastoquinone pool in the PSII regulates alternative splicing of many genes, especially splicing-related ones (Petrillo et al. 2014). Reactive oxygen species, singlet oxygen, which is produced by strong-light stress in the chloroplasts, causes cell death or stress acclimation (Ramel et al. 2012).

Levels of photosynthesis-assimilated carbons, sucrose and starch are finely regulated in close association with photosynthetic activity as well. Many plants, including *Arabidopsis thaliana*, accumulate starch in leaves in the day and degrade it in the night to maintain a carbon supply (Caspar et al. 1985, Gibon et al. 2004, Gibon et al. 2009, Streb and Zeeman 2012). In some plants, including major grains, sucrose is used as a main storage metabolite in leaves. Starch is synthesized as an overflow product from sucrose synthesis when carbon assimilation is vigorous, or in a regulated manner even during low photosynthesis, depending on the plant species. In the overflow model, a high level of sucrose causes photosynthates to be retained in the chloroplast and promotes their conversion into starch

(Stitt et al. 1983, Stitt and Heldt 1984). Genetic screens for starch-deficient mutants identified key enzymes for starch biosynthesis, such as plastidic phosphoglucomutase (PGM) and plastidic ADP-glucose pyrophosphorylase (AGPase) (Caspar et al. 1985, Lin et al. 1988). For regulated starch synthesis, light and sucrose induce redox-dependent activation of AGPase (Michalska et al. 2009). Sucrose phosphate synthase (SPS) is a key enzyme for sucrose synthesis. Reduction of SPS activity induces the accumulation of starch in rice (Hashida et al. 2016) and *A. thaliana* (Bahaji et al. 2015), and SPS overexpression in *A. thaliana* increases the sucrose/starch ratio (Signora et al. 1998). SPS activity is regulated by allosteric effectors and reversible phosphorylation (S.C. Huber and J.L. Huber 1992, J.L. Huber and S.C. Huber 1992, Huber and Huber 1996). Thus, carbon distribution between starch and sucrose is regulated at multiple steps, by metabolites as well as posttranslational modifications of enzymes, to accommodate photosynthesis activity changes.

For photosynthesis-dependent regulation of cellular processes, members of the Raf-like kinases have been shown to have relevant functions. Raf protein serine/threonine kinases were first identified in animals and function in transmitting growth factor-derived signals for cell proliferation (Daum et al. 1994). The genome of *A. thaliana* encodes 49 genes for protein kinases with a kinase domain homologous to those of the animal Raf kinases (MAPK Group 2002). Among them, HIGH LEAF TEMPERATURE 1 (HT1), BLUE LIGHT-DEPENDENT H⁺-ATPASE PHOSPHORYLATION (BHP) and CONVERGENCE OF BLUE LIGHT AND CO₂ 1 and 2 (CBC1 and 2) were reported to play roles in CO₂⁻ and/or blue-light (BL)-responsive stomatal movements (Hashimoto et al. 2006, Hayashi et al. 2017, Hiyama et al. 2017). In addition, other Raf-like kinases, STY8, 17 and 46 (for Ser/Thr/Tyr kinases), were shown to phosphorylate chloroplast transit peptides (Martin et al. 2006) and regulate chloroplast differentiation (Lamberti et al. 2011).

In this study, we aimed at identifying novel factors that mediate photosynthesis signaling in the liverwort *Marchantia polymorpha*, an extant bryophyte species in the basal lineage of land plants (Qiu et al. 2006, Puttick et al. 2018). The study of *M. polymorpha* is already providing clues to evolutionary origins, principles and conservation and divergence of various processes and their regulatory mechanisms during plant evolution, as exemplified by phytohormone and light signaling (Monte et al. 2018, Mutte et al. 2018, Inoue et al. 2019). Low genetic redundancy for most regulatory gene families in the genome and the availability of genetic information and efficient genetic tools (Ishizaki et al. 2013, Ishizaki et al. 2015, Ishizaki et al. 2016, Bowman et al. 2017, Sugano and Nishihama 2018, Sugano et al. 2018) make *M. polymorpha* suitable for systems biology approaches. In *M. polymorpha*, photosynthesis-derived sugar was shown to promote the first cell division of spores (Nakazato et al. 1999) and, in concert with a photoreceptor-derived signal, cell-cycle re-entry for regeneration (Nishihama et al. 2015), highlighting the importance of photosynthesis signaling in this species as well. By phosphoproteomic analysis, we identified a Raf-like kinase

as a protein subjected to photosynthesis-dependent phosphoregulation. Furthermore, genetic and physiological analyses revealed that the Raf-like kinase is important for plant growth and carbon metabolism. Our study provides an insight into the regulatory mechanisms of plant growth that are linked to photosynthesis.

Results

Identification of a Raf-like kinase that is phosphoregulated upon stimulation of photosynthesis

To identify novel factors that mediate photosynthesis signaling, we performed a phosphoproteomic analysis of dark-adapted or BL-irradiated *M. polymorpha* thalli with or without treatment with a photosynthesis inhibitor, DCMU, which significantly inhibited photosynthesis at concentrations of 10 μM or more (Supplementary Fig. S1 and Dataset S1). In *M. polymorpha*, a BL receptor phototropin (Mpphot) and plasma membrane H⁺-ATPases (MphAs) were shown to be phosphorylated in a BL- and photosynthesis-dependent manner, respectively (Okumura et al. 2012, Komatsu et al. 2014). Consistent with these previous reports, we detected phosphoregulation of Mpphot and MphA2 upon irradiation with BL, which was unaffected by DCMU and suppressed by DCMU, respectively (Supplementary Fig. S2), validating our experimental conditions and the phosphoproteomic dataset acquired.

We found many phosphopeptides whose levels varied with light irradiation only in the absence of DCMU treatment, like those of MphAs. Among them, we focused on a phosphopeptide derived from a protein kinase, Mapoly0013s0150, which exhibited a rapid change in its phosphorylation level as early as 10 min after light irradiation (Fig. 1A; Supplementary Dataset S1). Mapoly0013s0150 belongs to the B4 group of the Raf-like protein kinase family (Bowman et al. 2017), and we therefore designated it as PHOTOSYNTHESIS-RELATED RAF (MpPRAF), following the *Marchantia* nomenclature (Bowman et al. 2016). As with most B4 Raf-like kinases, MpPRAF consists of an N-terminal Phox and Bem1 (PB1) domain, a nonconserved middle region and a C-terminal kinase domain (Fig. 1B; Supplementary Fig. S3). No canonical sequences for a signal-peptide/transmembrane domain or a chloroplast-targeting signal are present in MpPRAF, based on the prediction programs SOSUI (Hirokawa et al. 1998) and ChloroP (Emanuelsson et al. 1999), suggesting cytosolic localization of MpPRAF. Ser-1248, which was predicted to be phosphorylated by the mass spectrometric analysis, is positioned in the nonconserved middle region just upstream of the kinase domain (Fig. 1B).

To further validate the photosynthesis-dependent phosphorylation of MpPRAF, we raised an antibody against a portion of the MpPRAF protein (amino acids 718–946; Fig. 1B); the antibody specifically detected two endogenous MpPRAF isoforms as two bands by immunoblotting (see Fig. 2A), which derive from splicing variants (Supplementary Fig. S4). Consistent with the results of the phosphoproteomic analysis, immunoblot analysis revealed a retardation of

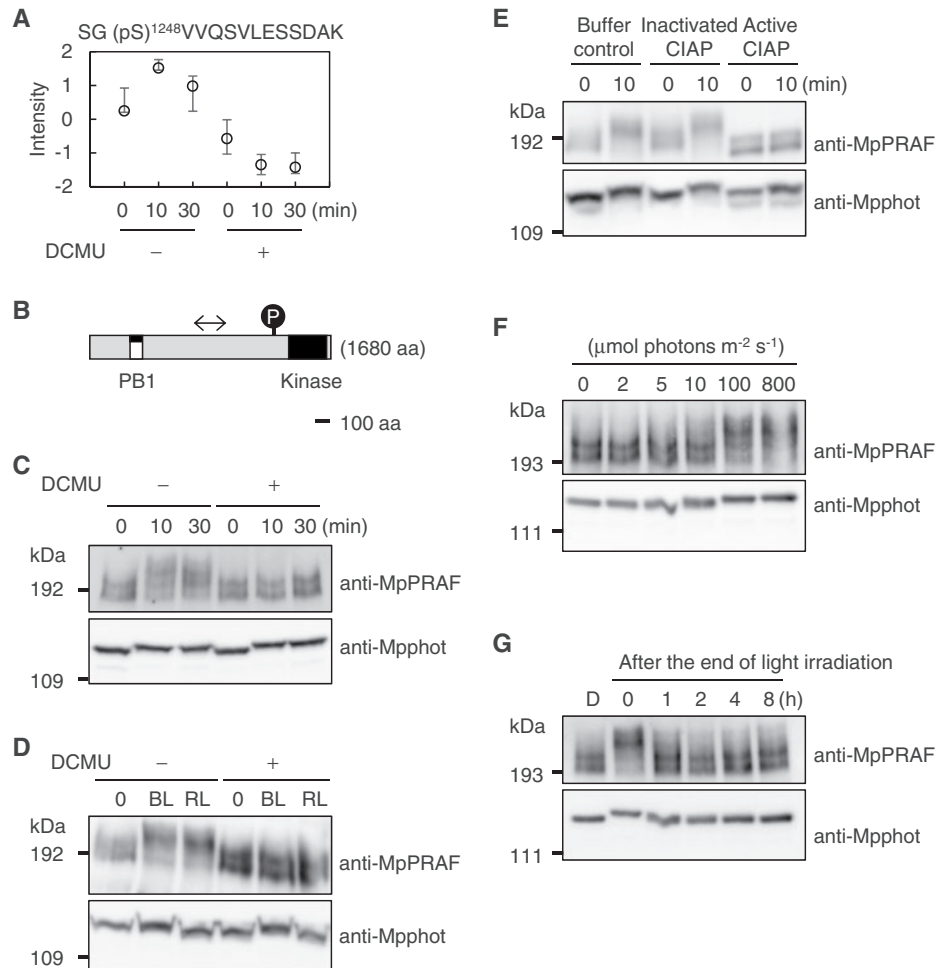


Fig. 1 Photosynthesis-dependent phosphorylation of a Raf-like kinase, MpPRAF. (A) Phosphorylation of MpPRAF detected by phosphoproteomic analysis. WT plants were grown under continuous white light for 7 d, transferred to darkness for 3 d in the presence (+) or absence (–) of 10 μM DCMU for the last day and then irradiated with BL (110 $\mu\text{mol photons m}^{-2} \text{s}^{-1}$) for 10 or 30 min. Quantified levels of Ser-1248 phosphorylation are plotted as the base 2 logarithm ($n = 3$ biologically independent experiments). Open circles and bars indicate medians and ranges of intensities, respectively. The identified and quantified phosphopeptide sequence is indicated above the plot. pS shows Ser-1248 that was predicted to be phosphorylated. (B) Schematic diagram of MpPRAF protein structure. The double-headed arrow and a filled circle represent the region used for antigen production and phosphorylated Ser-1248 identified by the phosphoproteomic analysis, respectively. (C, D) Immunoblot analysis with anti-MpPRAF antibody. Anti-Mpphot antibody (Komatsu et al. 2014) was used to show equal loading and effectiveness of BL. (C) DCMU-treated or untreated, dark-adapted plants, as in (A), were irradiated with BL (110 $\mu\text{mol photons m}^{-2} \text{s}^{-1}$). (D) DCMU-treated or untreated, dark-adapted plants, as in (A), were irradiated with either BL (110 $\mu\text{mol photons m}^{-2} \text{s}^{-1}$) or RL (80 $\mu\text{mol photons m}^{-2} \text{s}^{-1}$) for 10 min. (E) Loss of mobility shift by phosphatase treatment. Protein samples (irradiated with BL for 10 min, as in C) desalted by trichloroacetic acid/acetone precipitation were treated with active calf intestine alkaline phosphatase (CIAP), heat-inactivated CIAP or buffer, and subjected to immunoblot analysis. (F) Responsivity of MpPRAF phosphorylation to various light intensities. Dark-adapted plants, as in (A), were irradiated with BL (2, 5, 10, 100 or 800 $\mu\text{mol photons m}^{-2} \text{s}^{-1}$) for 10 min and subjected to immunoblot analysis. (G) Dephosphorylation of MpPRAF in the dark. WT plants were irradiated with BL (110 $\mu\text{mol photons m}^{-2} \text{s}^{-1}$) for 10 min, as in (C), transferred to darkness for 1, 2, 4 or 8 h, and subjected to immunoblot analysis.

MpPRAF protein mobility, to various degrees, on sodium dodecyl sulfate (SDS)–PAGE gels in response to irradiation with BL, but not in the presence of DCMU (Fig. 1C). In contrast, mobility retardation of Mpphot was detected regardless of DCMU treatment, confirming that the photosynthesis inhibitor treatment did not affect BL-triggered Mpphot phosphorylation responses. Moreover, red light (RL) also induced a mobility shift of MpPRAF, but not Mpphot (Fig. 1D). To confirm that the mobility shifts were caused by the phosphorylation of MpPRAF, we performed a phosphatase assay. After incubation with active phosphatase, but

not with heat-inactivated phosphatase, the light-induced mobility shifts of MpPRAF disappeared (Fig. 1E). These results suggest that MpPRAF becomes phosphorylated upon the stimulation of photosynthesis.

We further examined the responsiveness of MpPRAF phosphorylation to various light intensities. BL intensities over 100 $\mu\text{mol photons m}^{-2} \text{s}^{-1}$ induced clear mobility shifts of MpPRAF within 10 min, but weak light less than or equal to 10 $\mu\text{mol photons m}^{-2} \text{s}^{-1}$ did not (Fig. 1F). In contrast, Mpphot exhibited an intermediate mobility shift at 10 $\mu\text{mol photons m}^{-2} \text{s}^{-1}$ (Fig. 1F). We then compared phosphorylation levels

of MpPRAF during the process of dark adaptation. When BL-irradiated thalli were returned to the dark, the mobility of MpPRAF returned largely to that in nonirradiated thalli within 1 h (Fig. 1G). These results suggest that phosphorylation and dephosphorylation of MpPRAF occur reversibly in a light-dose-dependent manner.

Function of MpPRAF in growth optimization

To investigate the physiological roles of MpPRAF, we generated a knockout mutant of MpPRAF (*Mppraf*^{ko}) using homologous recombination (Ishizaki et al. 2013). The targeted disruption of the PB1-domain-coding region within MpPRAF was confirmed by genomic PCR (Supplementary Fig. S5A, B). However, immunoblotting with the anti-MpPRAF antibody revealed that the *Mppraf*^{ko} mutant produced truncated MpPRAF proteins (Fig. 2A). To obtain a complete null mutant, we generated a large-deletion mutant (*Mppraf*^Δ), in which the entire MpPRAF locus was deleted using clustered regularly interspaced short palindromic repeats (CRISPR)/CRISPR-associated endonuclease 9 (Cas9)-based genome editing (Supplementary Fig. S5C, D; Hisanaga et al. 2019), and no band was detected with the anti-MpPRAF antibody (Fig. 2A). Both *Mppraf*^{ko} and *Mppraf*^Δ mutants grew more slowly than wild-type (WT) plants (Fig. 2B); moreover, the slow-growth phenotype was rescued by introducing a genomic fragment containing the MpPRAF gene or a modified genomic fragment expressing only the short splicing variant (*MpPRAF*^{sv1}), both fused with 3xFLAG at its C-terminus (Fig. 2B, C; Supplementary Fig. S4E). Differences of fresh weight between WT and *Mppraf*^Δ plants became larger as the light intensity increased, up to 80 μmol photons m⁻² s⁻¹ (Supplementary Fig. S6). Fresh weight of WT plants did not further increase above 80 μmol photons m⁻² s⁻¹, which can be due to photoinhibition caused by strong light, in line with a previously published result that the amounts of chlorophyll and carotenoids decreased at high light intensity (226 μmol photons m⁻² s⁻¹) compared with low light (67.1 μmol photons m⁻² s⁻¹) in *M. polymorpha* (Soriano et al. 2019). These results suggest that MpPRAF plays an important role in optimizing growth. We used both *Mppraf*^{ko} and *Mppraf*^Δ for further experiments, as the truncated MpPRAF proteins expressed in *Mppraf*^{ko} were evidently not functional.

Hyper-accumulation of starch and reduction of sucrose in the absence of MpPRAF

Previous studies revealed that light/dark conditions affect phosphorylation levels of several key enzymes for sugar metabolism, including SPS, cytosolic AGPase and PGM, in *A. thaliana* (Boex-Fontvieille et al. 2014, Abadie et al. 2016). In our phosphoproteomic analysis with *M. polymorpha*, phosphopeptides from those enzymes were detected as well (Supplementary Dataset S1). We therefore quantified photosynthetic carbon metabolites, including starch, sucrose, glucose and fructose. In plants that were grown from gemmae for 15 d under continuous white light, we found that starch accumulated to a much higher level in the *Mppraf* mutants than in the WT (Fig. 3A).

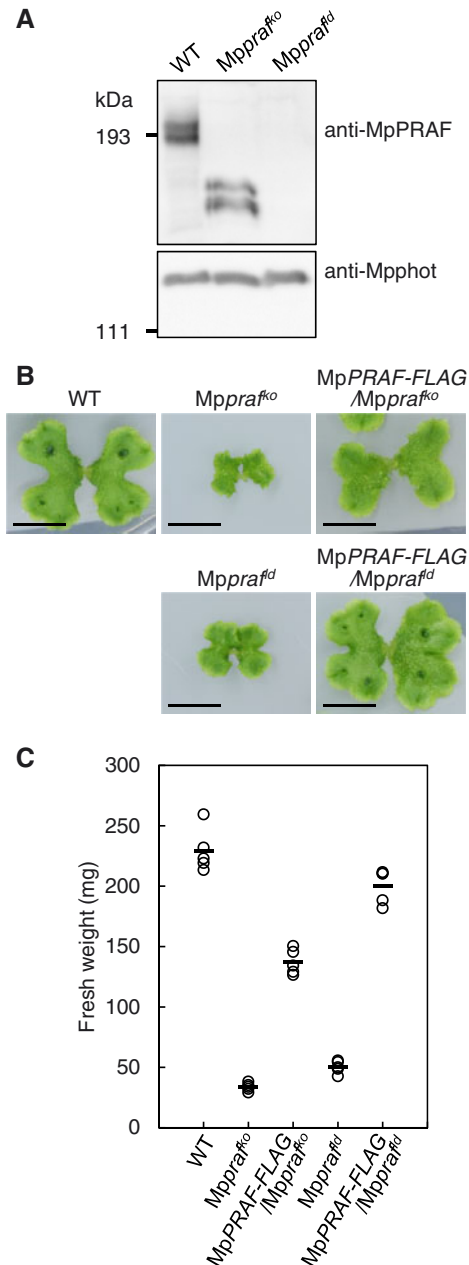


Fig. 2 *Mppraf* mutations cause growth retardation. (A) Immunoblot analysis with anti-MpPRAF using WT, *Mppraf*^{ko} and *Mppraf*^Δ plants grown under continuous white light for 7 d. Immunoblotting with anti-Mpphot (Komatsu et al. 2014) is shown as a loading control. (B) Photos of WT, *Mppraf*^{ko}, *proMpPRAF*:*MpPRAF*-3xFLAG/*Mppraf*^{ko} (*MpPRAF*-FLAG/*Mppraf*^{ko}), *Mppraf*^Δ and *proMpPRAF*:*MpPRAF*-3xFLAG/*Mppraf*^Δ (*MpPRAF*-FLAG/*Mppraf*^Δ) plants grown under continuous white light for 14 d. Bars = 1 cm. (C) Plot of fresh weight. The bars represent the averages of five biological replicates.

Conversely, sucrose levels in the *Mppraf* mutants were significantly lower, by about 5-fold, than those in the WT (Fig. 3A). There was no significant difference in the levels of glucose between the WT and *Mppraf* mutants, and the levels of fructose were slightly lower in *Mppraf* mutants compared with the WT (Fig. 3A; Supplementary Fig. S9B).

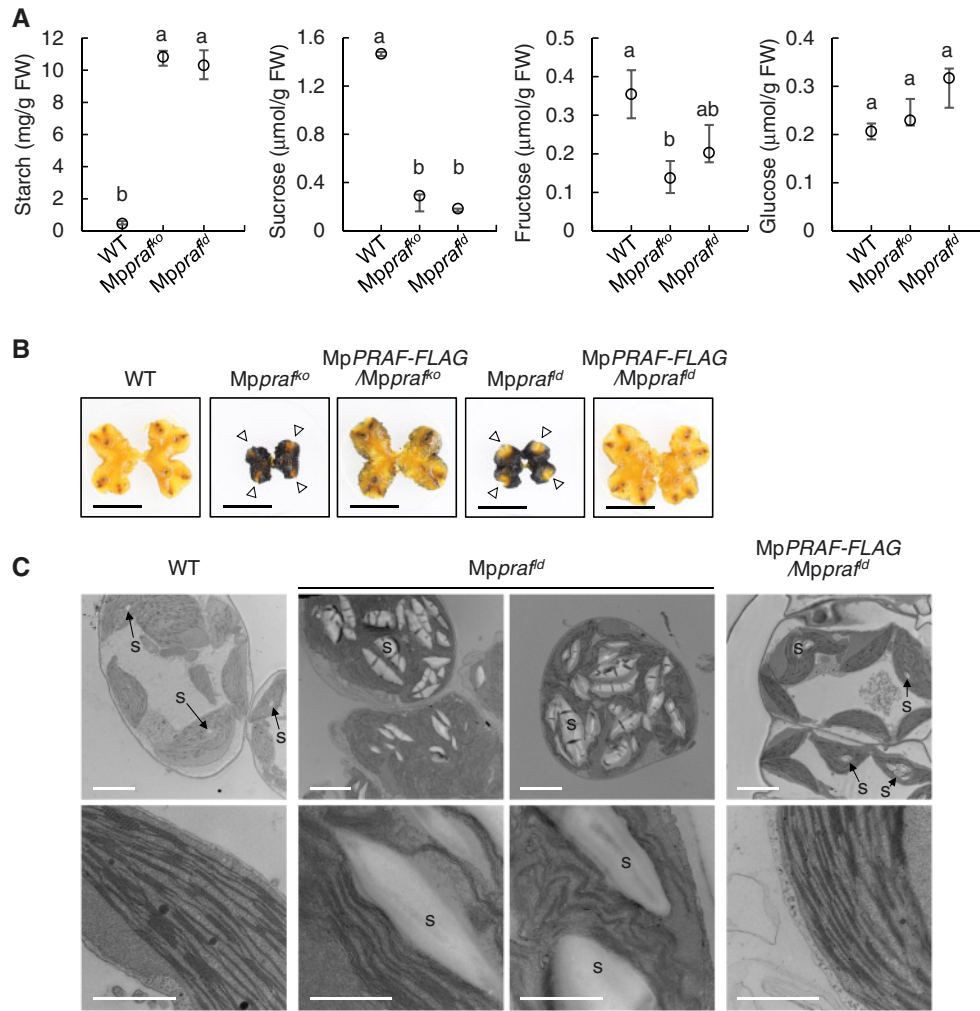


Fig. 3 Imbalance of starch and sugar contents in *Mppraf* mutants. (A) Quantification of starch, sucrose, glucose and fructose contents in WT, *Mppraf^{ko}* and *Mppraf^{dd}* plants grown under continuous white light for 15 d. Medians are plotted. Bars indicate ranges of biological replicates ($n = 3$), except for sucrose, glucose and fructose in WT ($n = 2$). Symbols above the bars indicate grouping by P -value < 0.05 in a Tukey–Kramer test. (B) Iodine staining of the indicated plants grown under continuous white light for 14 d. Arrowheads indicate the position of the meristem in *Mppraf^{ko}* and *Mppraf^{dd}* mutants. Bars = 1 cm. (C) TEM images of chloroplasts in assimilatory filament cells of the indicated plants grown under continuous white light for 14 d. Starch granules (s) are present in chloroplasts (only representative starch granules are labeled for *Mppraf^{dd}*). Bars = 5 μm (top); 1 μm (bottom).

Consistent with the starch quantification results, iodine staining showed the accumulation of starch in *Mppraf^{ko}* and *Mppraf^{dd}* mutants throughout the entire tissue except meristems, while essentially no starch staining was observed in the WT. The *Mppraf^{dd}* mutant accumulated starch even under weak light conditions at $10 \mu\text{mol photons m}^{-2} \text{ s}^{-1}$ (Supplementary Fig. S7), and the starch hyper-accumulation phenotype was rescued by re-introducing MpPRAF or MpPRAF^{sv1} to the mutant (Fig. 3B; Supplementary Figs S4F, S7). Transmission electron microscopy (TEM) analysis with 2-week-old plants revealed little accumulation of starch in chloroplasts of WT plants or the complemented line, whereas extremely large starch granules were observed in *Mppraf^{dd}* chloroplasts (Fig. 3C). These results suggest that MpPRAF plays a crucial role in partitioning between starch and sucrose.

MpPRAF is involved in growth control via regulation of sucrose metabolism

To examine whether the abnormal accumulation of starch is involved in the growth retardation of the *Mppraf* mutants, we attempted to introduce a starch-synthesis deficiency into the *Mppraf^{ko}* mutant background by disrupting an orthologous gene for a chloroplast-targeted PGM, a key enzyme for starch synthesis in *A. thaliana* (Caspar et al. 1985). BLAST searches against the *M. polymorpha* genome database identified one homolog, named MpPGM1 (Mapoly0202s0014), which is 79% identical to *A. thaliana* PGM1 (Supplementary Fig. S8A). We designed gRNA target sequences to disrupt the metal-binding site or catalytic reaction center, both important for the enzymatic activity (Periappuram et al. 2000), to generate mutant alleles of MpPGM1 by CRISPR/Cas9-based genome editing (Sugano and Nishihama 2018, Sugano et al. 2018). Genomic

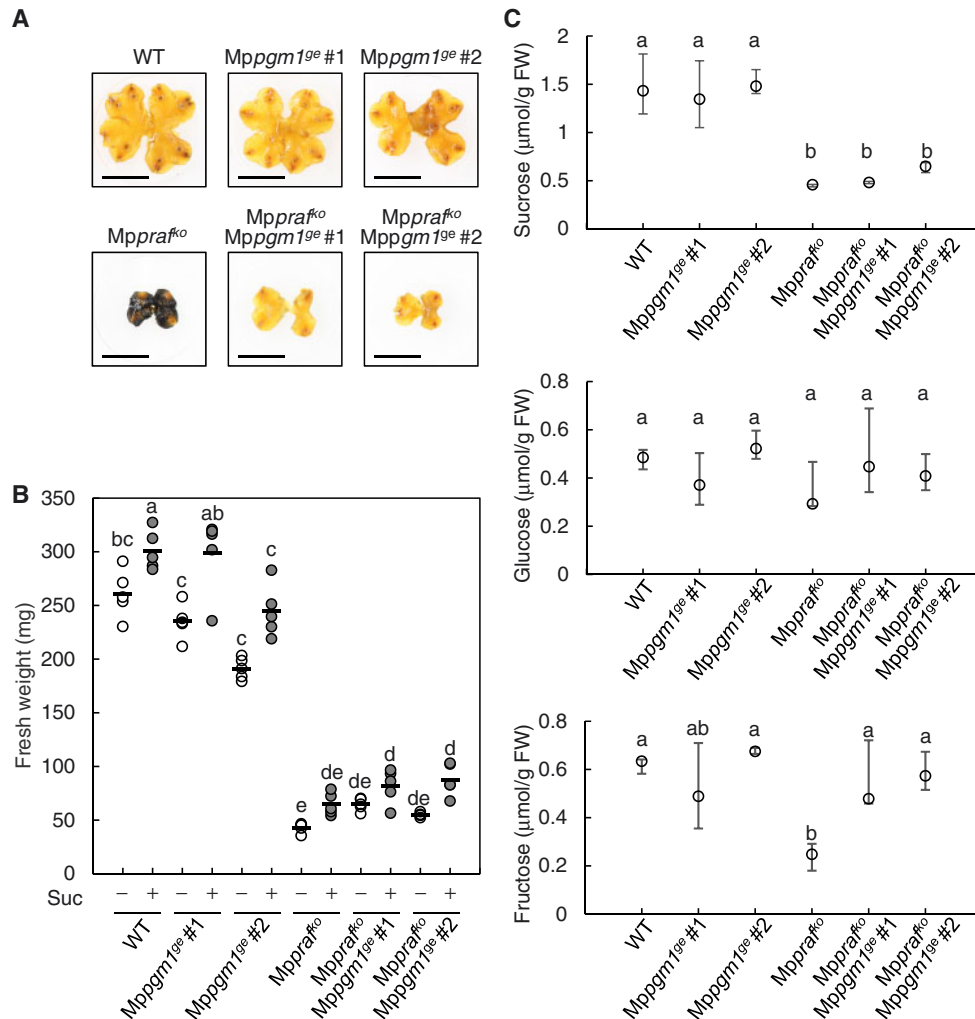


Fig. 4 Effects of *Mppgm1* mutations and exogenously supplied sucrose on *Mppraf* mutant phenotypes. (A) Iodine staining of WT, *Mppgm1^{se}*, *Mppraf^{ko}* and *Mppraf^{ko} Mppgm1^{se}* plants grown under continuous white light for 14 d in the absence of 1% sucrose. Bars = 1 cm. (B) Plot of fresh weight of the indicated plants grown under continuous white light for 14 d in the absence (–) or presence (+) of 1% sucrose. The bars represent the averages of five biological replicates. (C) Quantification of sucrose, fructose and glucose contents in WT, *Mppgm1^{se}*, *Mppraf^{ko}* and *Mppraf^{ko} Mppgm1^{se}* plants grown under continuous white light for 14 d in the absence of exogenously supplied sucrose. Bars indicate ranges of biological replicates ($n = 3$), except for sucrose in *Mppraf^{ko} Mppgm1^{se} #1* ($n = 2$). Symbols above the bars indicate grouping by significant differences ($P < 0.05$) in a Tukey–Kramer test.

PCR and direct sequencing analyses confirmed frame-shift mutations at the *MpPGM1* locus in both the *Mppraf^{ko}* and WT backgrounds (**Supplementary Fig. S8B**). As expected, mutations in *MpPGM1* suppressed starch hyper-accumulation in *Mppraf^{ko}* plants (**Fig. 4A**; **Supplementary Fig. S8C, E**), indicating that starch biosynthesis in the *Mppraf^{ko}* mutant occurred via *MpPGM1*. However, the slow-growth phenotype was not rescued by the *Mppgm1* mutations (**Fig. 4B**; **Supplementary Fig. S8D**), suggesting that starch accumulation was not the major cause of the observed slow-growth phenotype of the *Mppraf* mutants.

Because the elevated starch level was not the cause of the slow-growth phenotype, we examined the sugar content in the *Mppraf^{ko} Mppgm1^{se}* double mutants (**Fig. 4C**; **Supplementary Fig. S8E**). Single or combined mutations in *MpPRAF* and *MpPGM1* did not affect glucose content. Interestingly, however, sucrose content in the *Mppraf^{ko} Mppgm1^{se}* double mutants

remained low, similar to that in the *Mppraf^{ko}* single mutant. On the other hand, the fructose content in the double mutants was restored to the WT level. These results led us to examine whether a supply of sucrose could rescue the mutant phenotypes. Somewhat surprisingly, exogenous supplementation of sucrose only slightly restored the growth of *Mppraf* mutants, but the growth was still far below the WT level (**Fig. 4B**; **Supplementary Fig. S9A**). Furthermore, although exogenously supplied sucrose induced internal accumulation of sucrose in the WT, it did not occur in the *Mppraf* mutants (**Supplementary Fig. S9B**). While starch content in the WT and *Mppraf* plants was not affected by exogenously supplied sucrose, the levels of glucose and fructose were elevated by this treatment (**Supplementary Fig. S9B**). Taken together, these results suggest that the deficiency in endogenous production or accumulation of sucrose is associated with the slow-growth phenotype of the *Mppraf* mutants.

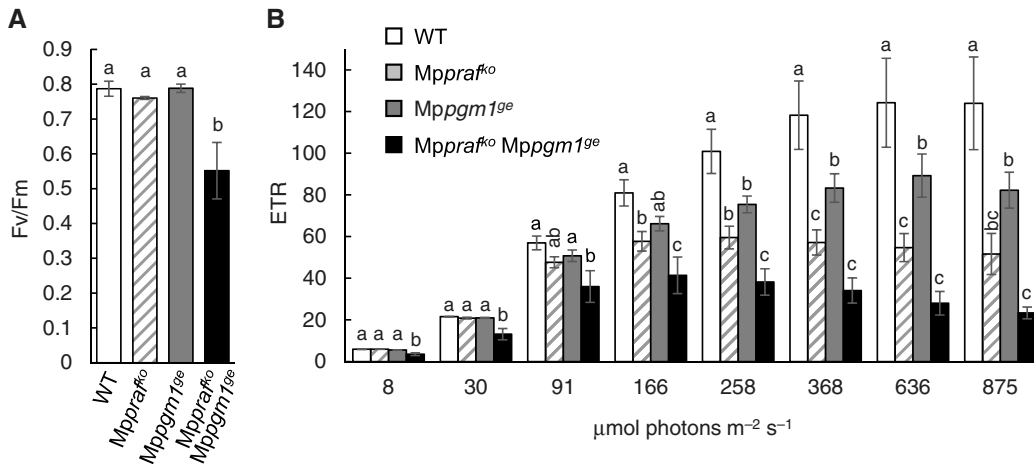


Fig. 5 Decreased electron transport in the absence of MpPRAF. (A) Fv/Fm and (B) ETR. WT, Mppraf^{ko}, Mppgm1^{ge} and Mppraf^{ko} Mppgm1^{ge} plants were grown under continuous white light for 14 d and transferred to darkness at least 30 min before chlorophyll fluorescence analysis. Means are plotted. Bars indicate SD ($n = 3$ biologically independent experiments). Symbols above the bars indicate grouping by P -value < 0.05 in a Tukey–Kramer test comparing WT, Mppraf^{ko}, Mppgm1^{ge} and Mppraf^{ko} Mppgm1^{ge} plants for respective light intensities.

Potential feedback defect in chloroplast electron transport in the absence of MpPRAF

As a previous study reported that a defect in photosynthetic carbohydrate metabolism negatively affects electron transport in the photosystems (Schmitz et al. 2012), we measured photosystem parameters by chlorophyll fluorescence analysis. Under the growth and light conditions in this study, WT and Mppraf^{ko} plants showed no difference in Fv/Fm (Fig. 5A), which is the maximum quantum efficiency of PSII and an indicator of damage to this photosystem (Butler and Kitajima 1975). However, the electron transport rate (ETR) (Munekage et al. 2001) was significantly compromised in Mppraf^{ko} plants. In the WT, ETR increased in a light-intensity-dependent manner up to $\sim 400 \mu\text{mol photons m}^{-2} \text{s}^{-1}$, where it reached saturation; in Mppraf^{ko}, ETR was significantly lower than in the WT above $166 \mu\text{mol photons m}^{-2} \text{s}^{-1}$ and became saturated at $\sim 200 \mu\text{mol photons m}^{-2} \text{s}^{-1}$ (Fig. 5B). These results demonstrate that Mppraf mutation negatively affects electron transport.

Interestingly, inhibition of starch synthesis by Mppgm1 mutation enhanced the photosystem defect in the Mppraf^{ko} mutant. Mppgm1 mutation itself had no effect on Fv/Fm, whereas combination of Mppraf^{ko} and Mppgm1 mutations synergistically decreased Fv/Fm (Fig. 5A), indicating that the double mutant caused photoinhibition of PSII under the growth conditions. Furthermore, ETR in the double mutant was lower than that of the respective single mutants (Fig. 5B). Given the synthetic effects between Mppraf^{ko} and Mppgm1 mutations on the photosystem parameters, the electron transport defect observed in the Mppraf^{ko} single mutant could be a secondary effect caused by a feedback regulation of electron transport from the photosynthate metabolism pathway.

Significance of Ser-1248 phosphorylation and kinase activity in MpPRAF function

Because our phosphoproteomic analysis detected photosynthesis-dependent phosphorylation of MpPRAF at

Ser-1248, we examined its physiological role. A mutated MpPRAF gene that had substitutions of both Ser-1248 and adjacent Ser-1246 to Ala (S1246AS1248A) was able to rescue the slow-growth and starch-accumulation defects of Mppraf^{ko} mutant (Supplementary Fig. S10A). Mobility shifts of MpPRAF^{S1246AS1248A} proteins were induced by light irradiation (Supplementary Fig. S10B). These results suggest that phosphorylation of MpPRAF at Ser-1248 and possibly Ser-1246 has little contribution to the observed MpPRAF functions in this study and indicate that MpPRAF has other photosynthesis-dependent phosphorylation sites. However, these results do not rule out the possibility that Ser-1248 phosphorylation plays significant roles in sugar metabolism under different growth conditions or in other processes that have not yet been investigated.

To gain insights into molecular functions of MpPRAF, we examined the significance of its kinase activity. Expression of a modified form of MpPRAF with an amino acid substitution of Asp-1540 to Asn (D1540N) (Supplementary Fig. S3B), a common kinase-dead mutation (Hanks and Hunter 1995, Porceddu et al. 2001, Komatsu et al. 2014), failed to rescue the slow-growth and starch-accumulation defects of the Mppraf^{ko} mutant (Fig. 6A, B). Moreover, no photosynthesis-induced mobility shift of MpPRAF^{D1540N} was observed (Fig. 6C), indicating that MpPRAF kinase activity is involved in its photosynthesis-induced phosphorylation. These data suggest that MpPRAF functions as a bona fide catalytically active kinase, and its kinase activity is required for the photosynthesis-induced responses.

Discussion

In this study, by using a phosphoproteomic approach, we identified a Raf-like kinase, MpPRAF, whose phosphorylation was induced in response to light irradiation. Effective phosphorylation by irradiation with either blue or RL and its block by photosynthesis inhibitor treatment demonstrate that

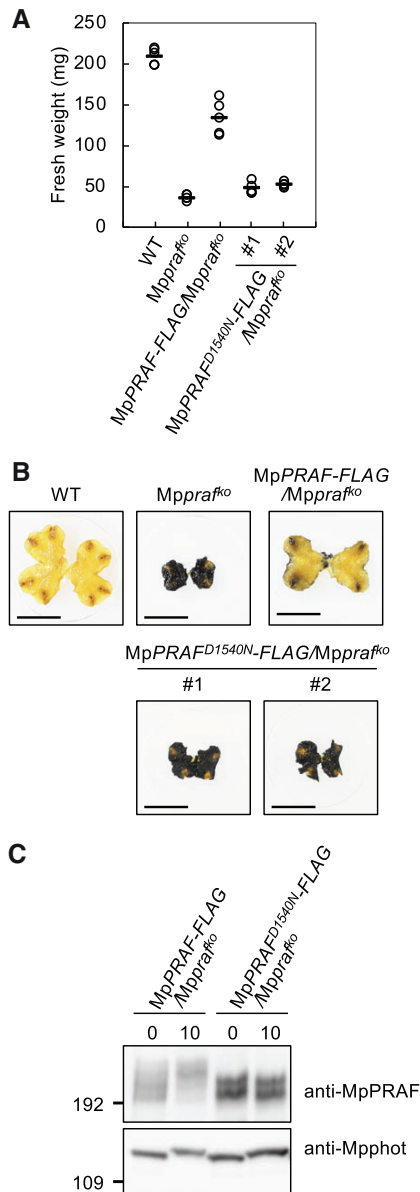


Fig. 6 Requirement of kinase activity for the function of MpPRAF. (A) Plot of fresh weight of WT, MpPRAF^{ko}, *pro*MpPRAF:MpPRAF-3xFLAG/MpPRAF^{ko} (MpPRAF-FLAG/MpPRAF^{ko}) and *pro*MpPRAF:MpPRAF^{D1540N}-3xFLAG/MpPRAF^{ko} (MpPRAF^{D1540N}-FLAG/MpPRAF^{ko}) plants grown under continuous white light for 14 d. The bars represent the averages of five biological replicates. (B) Iodine staining of the indicated plants in (A). Bars = 1 cm. (C) Immunoblot analysis with anti-MpPRAF antibody using the indicated plants grown under continuous white light for 7 d, transferred to the darkness for 3 d and then irradiated with BL (110 $\mu\text{mol photons m}^{-2} \text{s}^{-1}$) for 10 min. Anti-Mpphot antibody (Komatsu et al. 2014) was used to show equal loading and irradiation of BL.

MpPRAF phosphorylation is triggered by the stimulation of photosynthesis. Light-intensity-dependent phosphorylation of MpPRAF suggests a proportional relationship between the phosphorylation level and the photosynthetic activity.

Dephosphorylation of MpPRAF in the dark suggests that MpPRAF undergoes reversible phosphoregulation, consistent with the notion that the phosphorylation and dephosphorylation status corresponds to suitable and unsuitable environmental conditions for photosynthesis, respectively. As to which photosynthetic process serves as the stimulus for MpPRAF phosphorylation, at this moment, any photosynthetic processes downstream of the action point of DCMU, which blocks the binding of plastoquinones to PSII, are possible.

MpPRAF seemingly resides outside the chloroplast, as there is neither a chloroplast-targeting peptide nor a signal sequence/transmembrane domain in its sequence. Therefore, MpPRAF likely phosphorylates downstream targets in the cytosol. Because MpPRAF^{D1540N} was defective in its light-irradiation-induced band shifts, activation of MpPRAF is likely to be a prerequisite for its phosphorylation. Observed MpPRAF phosphorylation could be due to auto- or cross-phosphorylation or feedback phosphorylation by a downstream kinase activated by MpPRAF. It would be important to clarify whether the phosphorylation status of MpPRAF correlates with its kinase activity.

Mppraf mutants pleiotropically displayed growth retardation, accumulation of starch, decreased sucrose levels and electron transport defects, raising a question regarding which process MpPRAF primarily regulates. It should be noted that the Mppraf mutants accumulated starch even under the low light condition (10 $\mu\text{mol photons m}^{-2} \text{s}^{-1}$; **Supplementary Fig. S7**), where ETR was still at the WT level (**Fig. 5B**). Furthermore, Fv/Fm and ETR in the Mppraf^{ko} Mppgm1^{ge} double mutant, in which neither sucrose nor starch was accumulated much (**Fig. 4**; **Supplementary Fig. S8**), were more severely compromised than those in either of the single mutants (**Fig. 5**). These results suggest that the photosystem deficiency is a secondary effect, which was presumably caused by a defect in the photosynthate metabolism and subsequent negative-feedback regulation of electron transport. Such feedback regulation could occur, as is the case for *A. thaliana* plants with mutations in both TRIOSE PHOSPHATE/PHOSPHATE TRANSLOCATOR (TPT) and ADP-GLUCOSE PYROPHOSPHORYLASE 1 (ADG1) that are incapable of cytosolic carbohydrate synthesis (Schneider et al. 2002, Schmitz et al. 2012) and that exhibit growth retardation and defective photosynthetic electron transport (Hattenbach et al. 1997, Schneider et al. 2002, Häusler et al. 2009, Schmitz et al. 2012).

Our quantification, iodine staining and TEM analyses demonstrated hyper-accumulation of starch in Mppraf mutants (**Fig. 3**). However, starch hyper-accumulation does not seem to be responsible for the growth defect of Mppraf mutant, because the Mppraf Mppgm1 double mutants, in which starch synthesis was impaired, still showed growth retardation (**Fig. 4**; **Supplementary Fig. S8**). Interestingly, the intracellular sucrose level was not restored in the Mppraf Mppgm1 double mutants, either. Thus, MpPRAF might be primarily required for sucrose metabolism, and hyper-accumulation of starch, as well as decreased electron transport, in the Mppraf mutants would be a consequence of a sucrose-metabolism defect. This is consistent with a previous finding that severe reduction of sucrose

synthesis due to multiple mutations among the four isoforms of SPS genes in *A. thaliana* resulted in mutation-dose-dependent growth defects accompanied by hyper-accumulation of starch (Bahaji et al. 2015).

Neither the thallus growth defect nor the endogenous sucrose accumulation defect in *Mppraf* mutants was rescued by exogenously supplied sucrose (Fig. 4; Supplementary Fig. S9), which contrasts with the successful rescue of the aforementioned *A. thaliana tpt adg1* double mutants by exogenous supplementation with sucrose or glucose (Schmitz et al. 2012). The difference in the response of the *Mppraf* and *Atpt adg1* mutants to exogenously supplied sucrose implies that the *Mppraf* mutant phenotype is not solely caused by a defect in sucrose synthesis. Taken together, the failure to rescue the *Mppraf* growth defect and the increase in fructose or glucose in the *Mppraf* mutants by blocking starch synthesis or by exogenous sucrose treatment suggest roles of MpPRAF in both promoting sucrose synthesis and repressing sucrose catabolism.

While MpPRAF uniquely belongs to the B4 group of Raf-like kinases in *M. polymorpha* (Bowman et al. 2017), *A. thaliana* has seven B4 Raf-like kinases. Among them, the best-characterized is HCR1 (At3g24715), which was reported to regulate root hydraulic conductivity and hypoxia responsive gene expression (Shahzad et al. 2016). Two other B4 Raf-like kinases in *A. thaliana*, At1g16270 and At1g79570, were shown to be phosphorylated in response to osmotic stress (Stecker et al. 2014) and in a TOR-regulated manner (Van Leene et al. 2019), respectively, by phosphoproteomic analyses, although their physiological roles have not yet been elucidated. Our study raises the possibility that some B4 Raf-like kinases in vascular plants also play roles in photosynthesis signaling. At the same time, MpPRAF may function in signaling for other stimuli like hypoxia or osmotic stress in *M. polymorpha*. It is possible that B4 Raf-like kinases were neo/subfunctionalized in association with gene duplication during evolution. Further investigations will clarify the conservation and diversification of the B4 Raf-like kinase family.

In conclusion, we have identified the Raf-like kinase MpPRAF as a signaling factor that responds to a photosynthesis-derived stimulus and as a regulator of sucrose metabolism. Loss of MpPRAF function is presumed to primarily compromise sucrose accumulation, which in turn leads to starch hyperproduction. These abnormalities of photosynthate metabolism then could suppress electron transport in the photosystem as feedback regulation. Elucidation of activation mechanisms, identification of downstream targets and clarification of sub-cellular localization should provide a deeper understanding of MpPRAF functions.

Materials and Methods

Plant materials and growth conditions

Marchantia polymorpha accession, Takaragaike-1 (Tak-1) (Ishizaki et al. 2008), was used as WT. Tak-1 and mutants were cultured aseptically on half-strength Gamborg's B5 medium (Gamborg et al. 1968) containing 1% agar under 50–60 $\mu\text{mol photons m}^{-2} \text{s}^{-1}$ continuous white light with a cold cathode fluorescent lamp (OPT-40C-N-L, Optrom, Miyagi, Japan) at 22°C. F1 spores were obtained by crossing Tak-2 and Tak-1.

Light sources

BL and RL were given by a BL-emitting diode (LED) illuminator (MIL-B18, SANYO Electric; Osaka, Japan VBL-SD150-RB, Valore, Kyoto, Japan only for Fig. 1F) and red LED illuminator (MIL-R18, SANYO Electric), respectively. BL and RL intensities were measured by an 1830-C Optical Power Meter (Newport, Tokyo, Japan) and calculated at 450 and 657 nm, respectively. White light for Supplementary Fig. S6 was given by a cold cathode fluorescent lamp equipped with LH-80CCFL-6CT (NK System, Tokyo, Japan) for 10–80 $\mu\text{mol photons m}^{-2} \text{s}^{-1}$ or an LED illuminator (3LH-484; NK System) for 600 $\mu\text{mol photons m}^{-2} \text{s}^{-1}$. White light intensities were measured by an LA-105 light meter (NK System).

Generation of multiple sequence alignments

Homologs of MpPRAF were collected by BLASTP searches against *A. thaliana* (TAIR10), *Amborella trichopoda* (version 1.0), *Picea abies* (version 1.0), *Physcomitrella patens* (version 3.0) and *Klebsormidium nitens* (version 1.0) in MarpolBase (<http://marchantia.info/>, December 28, 2019, date last accessed) and against *Oryza sativa* in RAP-DB (<https://rapdb.dna.affrc.go.jp/tools/blast>, December 28, 2019, date last accessed). Multiple alignment of amino acid sequences of B4-group Raf-like kinases or PGM1 homologs was constructed using the MUSCLE program (Edgar 2004) implemented in Geneious software (version 6.1.8; Biomatters; <http://www.geneious.com/>, December 28, 2019, date last accessed) with default parameters. PB1 and kinase domains of B4-group Raf-like kinases were detected using SMART (Schultz et al. 1998) (<http://smart.embl-heidelberg.de>, December 28, 2019, date last accessed).

Generation of transgenic lines

To obtain the knockout line of MpPRAF, 5'- and 3'-homologous arms were amplified from the WT genomic DNA by PCR with the primer sets MpPRAF_GT5_F/MpPRAF_GT5_R and MpPRAF_GT3_F/MpPRAF_GT3_R, respectively. Primers used in this study are listed in Supplementary Table S1. The amplified 5'- and 3'-homologous arms were cloned into the *Ascl* and *Pacl* sites, respectively, of the pJHY-Tmp1 vector (Ishizaki et al. 2013) with an In-Fusion HD cloning kit (Takara, Shiga, Japan) to generate pJHY-Tmp1_MpPRAF, which was introduced into F1 sporelings by *Agrobacterium*-mediated transformation (Ishizaki et al. 2008). Screening of targeted lines was performed as described previously (Ishizaki et al. 2013). Gene-specific primers MpPRAF_GTcheck_F/MpPRAF_GTcheck_Rused in the screening are diagrammed in Supplementary Fig. S5.

To delete the entire MpPRAF gene locus, we exploited a nickase version of the CRISPR/Cas9 genome-editing system (Hisanaga et al. 2019). Pairs of gRNA target sequences were designed each in the upstream of the promoter and in the downstream of the transcriptional termination site of MpPRAF. Four sets of annealed oligo DNAs corresponding to the four gRNA sequences (MpPRAF_1A/MpPRAF_1B, MpPRAF_2A/MpPRAF_2B, MpPRAF_3A/MpPRAF_3B and MpPRAF_4A/MpPRAF_4B) were subcloned into the *BsaI* site of pMpGE-En04, pBC-GE12, pBC-GE23 and pBC-GE34, respectively, and the latter three gRNA expression cassettes were integrated further into the first plasmid. The resulting gRNA expression cassette array was transferred into pMpGE018 using the Gateway LR reaction to generate pMpGE018_MpPRAF. pMpGE-En04, pBC-GE12, pBC-GE23, pBC-GE34 and pMpGE018 were developed with Dr. Keisuke Inoue in Kyoto University. pMpGE018_MpPRAF was introduced into the WT using regenerating thalli as previously described (Kubota et al. 2013). For the identification of large-deletion mutant, gRNA-targeted regions were amplified from the genomic DNAs prepared from transformant thalli using the primer pairs MpPRAF_LDcheck_F/MpPRAF_KD_GT3_R. PCR products were directly sequenced with BigDye Terminator v3.1 (Thermo Fisher Scientific, Waltham, MA, USA) and the primers used for PCR.

To obtain the complementation lines of *Mppraf* mutants, genomic fragments containing a promoter or the coding sequence without the stop codon were amplified by PCR from Tak-1 genomic DNA with the primer sets MpPRAF_c5_F/MpPRAF_c5_R and MpPRAF_cds_F/MpPRAF_cds_R2, respectively. The amplified fragments were cloned into the pENTR/D-TOPO vector (Thermo Fisher Scientific). The *SfiI*-*Ascl* fragment carrying the promoter fragment from the first plasmid was cloned into the *SfiI* and *Ascl* sites of the second plasmid to generate pENTR/D-TOPO_MpPRAF. The combined sequence

containing the promoter and the coding region was then transferred to the pMpGWB309 vector (Ishizaki et al. 2015) using LR Clonase II (Thermo Fisher Scientific) to generate pMpGWB309_MpPRAF, which was introduced into the *Mppraf^{ko}* and *Mppraf^{td}* lines using regenerating thalli.

To construct mutated MpPRAF, site-directed mutagenesis was performed by PCR using pENTR/D-TOPO_MpPRAF as template. The primer sets used were MpPRAF_sv1_F/MpPRAF_sv1_R for MpPRAF^{sv1}, MpPRAF_S1246AS1248A_F/MpPRAF_S1246AS1248A_R for MpPRAF^{S1246AS1248A} and MpPRAF_D1540N_F/MpPRAF_gD1540N_R for MpPRAF^{D1540N}. The MpPRAF^{sv1} sequence was then transferred to the pMpGWB309 vector using LR Clonase II. The 5.6-kb *Bam*HI–*Bam*HI fragment of MpPRAF^{S1246AS1248A} and the 2.4-kb *Avr*II–*Avr*II fragment of MpPRAF^{D1540N} were ligated with the 16.6-kb *Bam*HI–*Bam*HI fragment and the 19.8-kb *Avr*II–*Avr*II fragment of pMpGWB309_MpPRAF, respectively. These vectors containing MpPRAF^{sv1}, MpPRAF^{S1246AS1248A} or MpPRAF^{D1540N} were introduced into the *Mppraf^{ko}* using regenerating thalli.

To obtain the mutant alleles of MpPGM1, gRNA oligo DNA sets MpPGM1_1A/MpPGM1_1B for catalytic center region and MpPGM1_2A/MpPGM1_2B5 for metal-binding site, respectively, were annealed, followed by ligation reactions with *Bsa*I-digested pMpGE_En03 vector (Sugano and Nishihama 2018, Sugano et al. 2018). The resulting constructs for catalytic center and metal-binding site were transferred to the pMpGE011 vector (Sugano and Nishihama 2018, Sugano et al. 2018) using LR Clonase II to generate pMpGE011_MpPGM1_1 and pMpGE011_MpPGM1_2, respectively. These vectors were introduced into the WT and *Mppraf^{ko}* plants using regenerating thalli. For the isolation of *Mppgm1* mutants, gRNA-targeted regions were amplified from genomic DNAs prepared from the thalli using the primer pairs MpPGM1_check_F/MpPGM1_check_R. PCR products were directly sequenced with BigDye Terminator v3.1 and the primer MpPGM1_check_F for PGM1_1 and MpPGM1_check_R for PGM1_2.

Phosphoproteomic analysis

To prepare samples for phosphoproteomic analysis, WT plants were grown on 9 cm plates under continuous white light (OPT-40C-N-L, 50–60 μmol photons m⁻² s⁻¹) for 7 d, transferred to the darkness for 3 d (dark treatment), irradiated with BL (MIL-B18, 110 μmol photons m⁻² s⁻¹) for 10 or 30 min and then frozen with liquid nitrogen. For DCMU-treated samples, 5 ml of 10 μM DCMU [0.1% (v/v) ethanol] was added to the plate in order to cover the medium surface on the second day of dark treatment, and the plate was incubated for one more day of dark treatment and then irradiated with BL for 10 or 30 min.

Frozen *M. polymorpha* gemmae were disrupted using a Shake Master Neo (Bio Medical Science, Tokyo, Japan). Powdered gemmae were immediately suspended in 4% SDS, 0.1 M Tris–HCl (pH 7.6), and incubated at 95°C for 3 min. The homogenate was centrifuged at 16,000 × g for 10 min, and the supernatant was collected. Protein concentration of the extract was determined using a bicinchoninic acid protein assay kit (Thermo Fisher Scientific), and the extract was digested by filter-aided sample preparation (FASP) method (Wiśniewski et al. 2009). Briefly, 60 μl of the protein extracts were diluted with 300 μl of 8 M urea, 0.1 M Tris–HCl (pH 8.5), and loaded on to Vivacon 500 (Sartorius Stedim Biotech, Göttingen, Germany). The proteins were reduced with 10 mM dithiothreitol for 30 min, alkylated with 50 mM iodoacetamide for 20 min at room temperature in the dark and digested with trypsin (1:100, w/w) overnight at 37°C on the filter, and then peptides were collected. The peptides were acidified with the addition of trifluoroacetic acid (TFA) and desalted using StageTips with C18 Empore disc membranes (3M, Maplewood, MN, USA) (Rappsilber et al. 2007), as described previously (Nakagami 2014). Phosphopeptides were enriched from the desalted samples by Ti-HAMMOC (Sugiyama et al. 2007), as described previously (Nakagami 2014). Briefly, the desalted tryptic digest from 400 μg of *M. polymorpha* protein was loaded onto custom-made HAMMOC tips with 3 mg of bulk titania (particle size, 10 μm; GL Sciences, Tokyo, Japan) for phosphopeptide enrichment. The enriched fraction was acidified with TFA, desalted using C18 StageTips and dried in a vacuum evaporator. The desalted peptides were dissolved in 9 μl of 5% acetonitrile containing 0.1% TFA for subsequent liquid chromatography-tandem mass spectrometry (LC–MS/MS) analysis.

An LTQ-Orbitrap XL (Thermo Fisher Scientific) coupled with an EASY-nLC 1000 (Thermo Fisher Scientific) was used for nano-LC–MS/MS analyses. A self-pulled needle (150-mm length × 100 μm i.d., 6 μm opening) packed with

ReproSil C18 materials (3 μm; Dr. Maisch GmbH, Ammerbuch, German) was used as an analytical column with a ‘stone-arch’ frit (Ishihama et al. 2002). A spray voltage of 2,400 V was applied. The injection volume was 6 μl, and the flow rate was 500 nl min⁻¹. The mobile phases consisted of 0.5% acetic acid and 2% acetonitrile (A) and 0.5% acetic acid and 80% acetonitrile (B). A three-step linear gradient of 5–10% B in 10 min, 10–40% B in 120 min, 40–95% B in 5 min and 95% B for 10 min was employed. The MS scan range was *m/z* 300–1,400. The top 10 precursor ions were selected in the MS scan by Orbitrap with resolution = 100,000 and for subsequent MS/MS scans by ion trap in the automated gain control mode, where automated gain control values of 5.00e+05 and 2.00e+05 were set for full MS and MS/MS, respectively. The normalized collision-induced dissociation was set to 35.0. A lock mass function was used for the LTQ-Orbitrap XL to obtain constant mass accuracy during gradient analysis (Olsen et al. 2005). Multi-stage activation was enabled upon detection of a neutral loss of phosphoric acid (98.00, 49.00 or 32.66 amu) (Schroeder et al. 2004) for further ion fragmentation. Selected sequenced ions were dynamically excluded for 30 s after sequencing.

Raw data were processed using MaxQuant software (version 1.6.3.4, <http://www.maxquant.org/>, December 28, 2019, date last accessed) (Cox and Mann 2008) with label-free quantification and iBAQ enabled (Tyanova et al. 2016a). MS/MS spectra were searched by the Andromeda search engine against a combined database containing the sequences from *M. polymorpha* (primary transcripts; http://marchantia.info/download/download/Mpolymorphav3.1.primaryTrs.pep_annot.fa.gz, December 28, 2019, date last accessed) and sequences of 248 common contaminant proteins and decoy sequences. Trypsin specificity was required, and a maximum of two missed cleavages allowed. Minimal peptide length was set to seven amino acids. Carbamidomethylation of cysteine residues was set as a fixed modification. Phosphorylation of serine, threonine and tyrosine residues, oxidation of methionine residue and protein N-terminal acetylation were set as variable modifications. Peptide-spectrum matches and proteins were retained if they were below a false discovery rate of 1%. Statistical analysis of the MaxLFQ values was carried out using Perseus (version 1.5.8.5, <http://www.maxquant.org/>, December 28, 2019, date last accessed) (Tyanova et al. 2016b).

Statistical analysis of the intensity values obtained for the phosphorylated sites [‘Phospho(STY)Sites.txt’ output file] was carried out using Perseus. Quantified sites were filtered for reverse hits, and then, the site table was expanded and intensity values were log₂-transformed. After grouping samples by treated conditions, sites that had three valid values in one of the conditions were retained for the subsequent analysis. Data were normalized by the subtraction of the median (matrix access = columns, subtract = median). Missing values were imputed from a normal distribution using the default settings in Perseus (width = 0.3, downshift = 1.8, separately for each column). Two-sample *t*-tests were performed using a permutation-based false discovery rate (FDR) of 5%. The Perseus output was exported and further processed using Excel. The data were deposited to jPOST (accession number: JPST000685; Okuda et al. 2017).

Production of anti-MpPRAF antibody

For the production of the anti-MpPRAF antibody, cDNA fragments for a non-conserved region of MpPRAF including amino acids 718–946 as the antigen were amplified by PCR with a primer set MpPRAF_antigen_F/MpPRAF_antigen_R from a MpPRAF cDNA, which had been amplified by reverse transcription-PCR from WT mRNA with the primer set MpPRAF_cds_F/MpPRAF_cds_R1 and cloned into the pENTR/D-TOPO vector. RNA extraction and reverse transcription were performed as described previously (Inoue et al. 2016). The amplified fragment for MpPRAF^{718–946} was cloned into the *Nde*I–*Xba*I fragment of an expression vector, pIN055 (kindly provided by Keisuke Inoue in Kyoto University), to fuse with a maltose-binding protein (MBP) tag at the N-terminus and a 6xHis affinity tag at the C-terminus, with an In-Fusion HD cloning kit. MBP-MpPRAF^{718–946}-6xHis protein was expressed in *Escherichia coli* strain Rosetta2(DE3) by induction with 0.1 mM isopropyl-β-D-thiogalactopyranoside for 24 h at 15°C. Cells were collected by centrifugation and resuspended in a lysis buffer containing 20 mM Tris–HCl (pH 8), 150 mM NaCl, 10% glycerol, 1 mM phenylmethylsulfonyl fluoride and 1 mM dithiothreitol. After the cells were lysed by sonication, the recombinant proteins in the supernatants were purified by affinity chromatography using amylose resin (New England Biolabs, Ipswich, MA, USA). The MBP tag was removed with PreScission Protease (GE Healthcare, Life Sciences, Buckinghamshire, UK).

MpPRAF^{718–946}-6xHis was purified by affinity chromatography using cOmplete His-Tag Purification Resin (Roche, Basel, Switzerland) and was used for raising the rabbit polyclonal antibody (KIWA Laboratory Animals, Wakayama, Japan). Filtrate of anti-MpPRAF serum through 0.45 µm membrane (Pall Corporation, Port Washington, NY, USA) was used as anti-MpPRAF antibody.

Protein extraction and immunoblot analysis

Seven-day-old plants were transferred to the darkness for 3 d. After DCMU treatment and/or various kinds of light irradiation indicated in the legends, plants were frozen and ground to a fine powder in a mortar with liquid nitrogen. The homogenates were mixed with equal volumes of a 2× SDS sample buffer [0.25 M Tris-HCl (pH 6.8), 10% (v/v) 2-mercaptoethanol, 4% (w/v) SDS, 10% (w/v) sucrose and 0.004% (w/v) bromophenol blue] and incubated at 95°C for 5 min, followed by centrifugation at 10,000 × g for 15 min. The supernatants were separated by SDS-PAGE on a 4% (w/v) acrylamide gel for MpPRAF and 5% or 6% acrylamide gel for Mpphot and transferred onto polyvinylidene fluoride membranes (Bio-Rad Laboratories, Hercules, CA, USA). For primary antibodies, anti-MpPRAF antibody (see above) and anti-Mpphot antibody (Komatsu et al. 2014) were diluted at 1:1,000 and 1:5,000, respectively. For the secondary antibody, Anti-Rabbit IgG, HRP-linked whole Ab (GE Healthcare Life Sciences) was diluted at 1:10,000. Blots were visualized with ECL Prime reagent (GE Healthcare Life Sciences) and ImageQuant LAS 4010 (GE Healthcare Life Sciences).

Phosphatase assay

Protein extracts were desalted by trichloroacetic acid precipitation. Equal amount of 20% (w/v) trichloroacetic acid was added to protein samples, which were incubated at 4°C for 30 min and centrifuged at 15,000 × g for 10 min at 4°C. The pellets were washed with cold acetone, centrifuged at 15,000 × g for 10 min at 4°C, dried up and suspended in calf intestine alkaline phosphatase (CIAP) buffer attached to CIAP enzyme (Takara). The desalted protein samples were incubated with heat-inactivated CIAP, which were incubated with equal volume of 10 mM EDTA at 65°C for 30 min, or active CIAP at 37°C for 1 h. Reactions were stopped by incubation with the 2× SDS sample buffer at 95°C for 5 min. Then, the samples were used for immunoblotting.

Chlorophyll fluorescence analysis

Chlorophyll fluorescence was measured in 14-day-old plants using a MINI-PAM portable chlorophyll fluorometer (Walz, Effeltrich, Germany). According to the previous report (Maxwell and Johnson 2000), Fv/Fm and Φ_{PSII} were calculated by the equations $(F_m - F_o)/F_m$ and $(F_m' - F_s)/F_m'$, respectively. The ETR was calculated as $\Phi_{PSII} \times PFD$ (photon flux density) (Munekage et al. 2001).

Quantification of starch, sucrose, glucose and fructose

Plants (~50 mg fresh weight) were lyophilized by Freezone 2.5 (LABCONCO, Kansas City, MO, USA), ground into a fine powder by shaking for 1 min with a metal cone in a collection tube using a Multi-Beads Shocker (Yasui Kikai, Osaka, Japan) and extracted twice in 0.5 ml of 80% (v/v) boiling ethanol for 5 min. Samples were then centrifuged at 12,000 × g for 15 min at 15°C. The pellets and supernatants were dried up. Then, starch in the pellet was extracted by boiling for 30 min in 1 ml of 0.2 M KOH. Two hundred microliter of 1 M acetic acid was added to the extract to adjust the pH to 5.5. The starch levels were determined by TOTAL STARCH Assay Kit (AMYLOGUCOSIDASE/ α -AMYLASE METHOD; Megazyme, Dublin, Ireland). The dried supernatants were suspended in 0.2 ml of water. Aliquots of the samples were then assayed for glucose, fructose and sucrose content using coupled enzymatic assay methods using SUCROSE, D-FRUCTOSE and D-GLUCOSE assay Kit (Megazyme).

Iodine staining

Plant samples were incubated with 80% (v/v) ethanol and 0.1% (v/v) 2-mercaptoethanol at 80°C for decolorization. Iodine staining was then performed as described by Hostettler et al. (2011). The decolorized plants were stained with Lugol solution [0.34% (w/v) I_2 and 0.68% (w/v) KI] for 5 min and washed twice with water for 2 min.

TEM analysis

Basal parts of the thallus were collected from 14-day-old plants and fixed with 2.5% (v/v) glutaraldehyde and 2% (w/v) paraformaldehyde in 50 mM phosphate buffer (pH 7.2) at 4°C overnight. After washing with 50 mM phosphate buffer, the samples were post-fixed with 2% (w/v) osmium tetroxide at room temperature for 2 h, dehydrated in a graded series of ethanol [25%, 50%, 80%, 99% and 100% (v/v)] and embedded in epoxy resin. Ultra-thin sections (80-nm thick) were cut with a diamond knife using an ultramicrotome (Ultracut UCT; Leica, Wetzlar, Germany), mounted on copper grids and stained with 2% (w/v) uranyl acetate and a lead stain solution. Samples were observed with transmission electron microscopes (H-7650, Hitachi High-Technologies, Tokyo, Japan; JEM-1011; JEOL, Tokyo, Japan).

Supplementary Data

Supplementary data are available at PCP online.

Acknowledgments

The authors thank Toshiharu Shikanai for the use of a MINI-PAM device and helpful discussions; Kentaro Ifuku for the use of a high-intensity-light chamber and helpful discussions; Hideya Fukuzawa, Masataka Kajikawa and Haruka Shinkawa for assistance with carbohydrate quantification; Keisuke Inoue for providing plasmids for large deletions and protein expression; Mika Terai and Asuka Shintaku for providing unpublished data that stimulated this research; and Keiko Okamoto-Furuta, Haruyasu Kohda, Yasuko Koumoto and Tomoo Shimada for technical assistance in electron microscopy. Finally, they thank anonymous reviewers for giving comments to improve the article.

Funding

The Japan Society for the Promotion of Science KAKENHI [24570048 to R.N.]; the Ministry of Education, Culture, Sports, Science & Technology KAKENHI [25113009 to T.K. and 18H04836 to R.N.]; and Max-Planck-Gesellschaft to H.N.

Disclosures

The authors have no conflicts of interest to declare.

References

- Abadie, C., Mainguet, S., Davanture, M., Hodges, M., Zivy, M. and Tcherkez, G. (2016) Concerted changes in the phosphoproteome and metabolome under different CO₂/O₂ gaseous conditions in Arabidopsis rosettes. *Plant Cell Physiol.* 57: 1544–1556.
- Bahaji, A., Baroja-Fernández, E., Ricarte-Bermejo, A., Sánchez-López, Á.M., Muñoz, F.J., Romero, J.M., et al. (2015) Characterization of multiple SPS knockout mutants reveals redundant functions of the four Arabidopsis sucrose phosphate synthase isoforms in plant viability, and strongly indicates that enhanced respiration and accelerated starch turnover can alleviate the blockage of sucrose biosynthesis. *Plant Sci.* 238: 135–147.
- Boex-Fontvieille, E., Davanture, M., Jossier, M., Zivy, M., Hodges, M. and Tcherkez, G. (2014) Photosynthetic activity influences cellulose biosynthesis and phosphorylation of proteins involved therein in Arabidopsis leaves. *J. Exp. Bot.* 65: 4997–5010.

- Bowman, J.L., Araki, T., Arteaga-Vazquez, M.A., Berger, F., Dolan, L., Haseloff, J., et al. (2016) The naming of names: guidelines for gene nomenclature in *Marchantia*. *Plant Cell Physiol.* 57: 257–261.
- Bowman, J.L., Kohchi, T., Yamato, K.T., Jenkins, J., Shu, S., Ishizaki, K., et al. (2017) Insights into land plant evolution garnered from the *Marchantia polymorpha* genome. *Cell* 171: 287–304.e15.
- Butler, W.L. and Kitajima, M. (1975) Energy transfer between photosystem II and photosystem I in chloroplasts. *Biochim. Biophys. Acta* 396: 72–85.
- Caspar, T., Huber, S.C. and Somerville, C. (1985) Alterations in growth, photosynthesis, and respiration in a starchless mutant of *Arabidopsis thaliana* (L.) deficient in chloroplast phosphoglucomutase activity. *Plant Physiol.* 79: 11–17.
- Cox, J. and Mann, M. (2008) MaxQuant enables high peptide identification rates, individualized p.p.b.-range mass accuracies and proteome-wide protein quantification. *Nat. Biotechnol.* 26: 1367–1372.
- Daum, G., Eisenmann-Tappe, I., Fries, H.W., Troppmair, J. and Rapp, U.R. (1994) The ins and outs of Raf kinases. *Trends Biochem. Sci.* 19: 474–480.
- Duby, G. and Boutry, M. (2009) The plant plasma membrane proton pump ATPase: a highly regulated P-type ATPase with multiple physiological roles. *Pflügers Arch.* 457: 645–655.
- Edgar, R.C. (2004) MUSCLE: multiple sequence alignment with high accuracy and high throughput. *Nucleic Acids Res.* 32: 1792–1797.
- Emanuelsson, O., Nielsen, H. and von Heijne, G. (1999) ChloroP, a neural network-based method for predicting chloroplast transit peptides and their cleavage sites. *Protein Sci.* 8: 978–984.
- Gamborg, O.L., Miller, R.A. and Ojima, K. (1968) Nutrient requirements of suspension cultures of soybean root cells. *Exp. Cell Res.* 50: 151–158.
- Gibon, Y., Bläsing, O.E., Palacios-Rojas, N., Pankovic, D., Hendriks, J.H., Fisahn, J., et al. (2004) Adjustment of diurnal starch turnover to short days: depletion of sugar during the night leads to a temporary inhibition of carbohydrate utilization, accumulation of sugars and post-translational activation of ADPglucose pyrophosphorylase in the following light period. *Plant J.* 39: 847–862.
- Gibon, Y., Pyl, E.T., Sulpice, R., Lunn, J.E., Höhne, M., Günther, M., et al. (2009) Adjustment of growth, starch turnover, protein content and central metabolism to a decrease of the carbon supply when *Arabidopsis* is grown in very short photoperiods. *Plant Cell Environ.* 32: 859–874.
- Hanks, S.K. and Hunter, T. (1995) Protein kinases 6. The eukaryotic protein kinase superfamily: kinase (catalytic) domain structure and classification. *FASEB J.* 9: 576–596.
- Hashida, Y., Hirose, T., Okamura, M., Hibara, K., Ohsugi, R. and Aoki, N. (2016) A reduction of sucrose phosphate synthase (SPS) activity affects sucrose/starch ratio in leaves but does not inhibit normal plant growth in rice. *Plant Sci.* 253: 40–49.
- Hashimoto, M., Negi, J., Young, J., Israelsson, M., Schroeder, J.I. and Iba, K. (2006) *Arabidopsis* HT1 kinase controls stomatal movements in response to CO₂. *Nat. Cell Biol.* 8: 391–397.
- Hattenbach, A., Muller-Rober, B., Nast, G. and Heineke, D. (1997) Antisense repression of both ADP-glucose pyrophosphorylase and triose phosphate translocator modifies carbohydrate partitioning in potato leaves. *Plant Physiol.* 115: 471–475.
- Häusler, R.E., Geimer, S., Kunz, H.H., Schmitz, J., Dörmann, P., Bell, K., et al. (2009) Chlororespiration and grana hyperstacking: how an *Arabidopsis* double mutant can survive despite defects in starch biosynthesis and daily carbon export from chloroplasts. *Plant Physiol.* 149: 515–533.
- Hayashi, M., Inoue, S., Ueno, Y. and Kinoshita, T. (2017) A Raf-like protein kinase BHP mediates blue light-dependent stomatal opening. *Sci. Rep.* 7: 45586.
- Hirokawa, T., Boon-Chieng, S. and Mitaku, S. (1998) SOSUI: classification and secondary structure prediction system for membrane proteins. *Bioinformatics* 14: 378–379.
- Hisanaga, T., Okahashi, K., Yamaoka, S., Kajiwar, T., Nishihama, R., Shimamura, M., et al. (2019) A cis-acting bidirectional transcription switch controls sexual dimorphism in the liverwort. *EMBO J.* 38: e100240.
- Hiyama, A., Takemiya, A., Munemasa, S., Okuma, E., Sugiyama, N., Tada, Y., et al. (2017) Blue light and CO₂ signals converge to regulate light-induced stomatal opening. *Nat. Commun.* 8: 1284.
- Hostettler, C., Kölling, K., Santelia, D., Streb, S., Kötting, O. and Zeeman, S.C. (2011) Analysis of starch metabolism in chloroplasts. *Methods Mol. Biol.* 775: 387–410.
- Huber, S.C. and Huber, J.L. (1992) Role of sucrose-phosphate synthase in sucrose metabolism in leaves. *Plant Physiol.* 99: 1275–1278.
- Huber, J.L. and Huber, S.C. (1992) Site-specific serine phosphorylation of spinach leaf sucrose-phosphate synthase. *Biochem. J.* 283: 877–882.
- Huber, S.C. and Huber, J.L. (1996) Role and regulation of sucrose-phosphate synthase in higher plants. *Annu. Rev. Plant Physiol. Plant Mol. Biol.* 47: 431–444.
- Inoue, K., Nishihama, R., Araki, T. and Kohchi, T. (2019) Reproductive induction is a far-red high irradiance response that is mediated by phytochrome and PHYTOCHROME INTERACTING FACTOR in *Marchantia polymorpha*. *Plant Cell Physiol.* 60: 1136–1145.
- Inoue, K., Nishihama, R., Kataoka, H., Hosaka, M., Manabe, R., Nomoto, M., et al. (2016) Phytochrome signaling is mediated by PHYTOCHROME INTERACTING FACTOR in the liverwort *Marchantia polymorpha*. *Plant Cell* 28: 1406–1421.
- Ishihama, Y., Rappsilber, J., Andersen, J.S. and Mann, M. (2002) Microcolumns with self-assembled particle frits for proteomics. *J. Chromatogr. A* 979: 233–239.
- Ishizaki, K., Chiyoda, S., Yamato, K.T. and Kohchi, T. (2008) *Agrobacterium*-mediated transformation of the haploid liverwort *Marchantia polymorpha* L., an emerging model for plant biology. *Plant Cell Physiol.* 49: 1084–1091.
- Ishizaki, K., Johzuka-Hisatomi, Y., Ishida, S., Iida, S. and Kohchi, T. (2013) Homologous recombination-mediated gene targeting in the liverwort *Marchantia polymorpha*. *Sci. Rep.* 3: 1532.
- Ishizaki, K., Nishihama, R., Ueda, M., Inoue, K., Ishida, S., Nishimura, Y., et al. (2015) Development of gateway binary vector series with four different selection markers for the liverwort *Marchantia polymorpha*. *PLoS One* 10: e0138876.
- Ishizaki, K., Nishihama, R., Yamato, K.T. and Kohchi, T. (2016) Molecular genetic tools and techniques for *Marchantia polymorpha* research. *Plant Cell Physiol.* 57: 262–270.
- Kircher, S. and Schopfer, P. (2012) Photosynthetic sucrose acts as cotyledon-derived long-distance signal to control root growth during early seedling development in *Arabidopsis*. *Proc. Natl. Acad. Sci. USA* 109: 11217–11221.
- Komatsu, A., Terai, M., Ishizaki, K., Suetsugu, N., Tsuboi, H., Nishihama, R., et al. (2014) Phototropin encoded by a single-copy gene mediates chloroplast photorelocation movements in the liverwort *Marchantia polymorpha*. *Plant Physiol.* 166: 411–427.
- Kubota, A., Ishizaki, K., Hosaka, M. and Kohchi, T. (2013) Efficient *Agrobacterium*-mediated transformation of the liverwort *Marchantia polymorpha* using regenerating thalli. *Biosci. Biotechnol. Biochem.* 77: 167–172.
- Lamberti, G., Gugel, I.L., Meurer, J., Soll, J. and Schwenkert, S. (2011) The cytosolic kinases STY8, STY17, and STY46 are involved in chloroplast differentiation in *Arabidopsis*. *Plant Physiol.* 157: 70–85.
- Lin, T., Caspar, T., Somerville, C. and Preiss, J. (1988) Isolation and characterization of a starchless mutant of *Arabidopsis thaliana* (L.) Heynh lacking ADPglucose pyrophosphorylase activity. *Plant Physiol.* 86: 1131–1135.
- MAPK Group (2002) Mitogen-activated protein kinase cascades in plants: a new nomenclature. *Trends Plant Sci.* 7: 301–308.
- Martin, T., Sharma, R., Sippel, C., Waagemann, K., Soll, J. and Voithknecht, U. C. (2006) A protein kinase family in *Arabidopsis* phosphorylates chloroplast precursor proteins. *J. Biol. Chem.* 281: 40216–40223.
- Mason, M.G., Ross, J.J., Babst, B.A., Wienclaw, B.N. and Beveridge, C.A. (2014) Sugar demand, not auxin, is the initial regulator of apical dominance. *Proc. Natl. Acad. Sci. USA* 111: 6092–6097.
- Maxwell, K. and Johnson, G.N. (2000) Chlorophyll fluorescence—a practical guide. *J. Exp. Bot.* 51: 659–668.
- Michalska, J., Zaubner, H., Buchanan, B.B., Cejudo, F.J. and Geigenberger, P. (2009) NTRC links built-in thioredoxin to light and sucrose in regulating

- starch synthesis in chloroplasts and amyloplasts. *Proc. Natl. Acad. Sci. USA* 106: 9908–9913.
- Monte, I., Ishida, S., Zamarreño, A.M., Hamberg, M., Franco-Zorrilla, J.M., García-Casado, G., et al. (2018) Ligand-receptor co-evolution shaped the jasmonate pathway in land plants. *Nat. Chem. Biol.* 14: 480–488.
- Munekage, Y., Takeda, S., Endo, T., Jahns, P., Hashimoto, T. and Shikanai, T. (2001) Cytochrome *b6f* mutation specifically affects thermal dissipation of absorbed light energy in *Arabidopsis*. *Plant J.* 28: 351–359.
- Mutte, S.K., Kato, H., Rothfels, C., Melkonian, M., Wong, G.K.S. and Weijers, D. (2018) Origin and evolution of the nuclear auxin response system. *eLife* 7: 1–25.
- Nakagami, H. (2014) StageTip-based HAMMOG, an efficient and inexpensive phosphopeptide enrichment method for plant shotgun phosphoproteomics. *Methods Mol. Biol.* 1072: 595–607.
- Nakazato, T., Kadota, A. and Wada, M. (1999) Photoinduction of spore germination in *Marchantia polymorpha* L. is mediated by photosynthesis. *Plant Cell Physiol.* 40: 1014–1020.
- Negi, J., Munemasa, S., Song, B., Tadakuma, R., Fujita, M., Azoulay-Shemer, T., et al. (2018) Eukaryotic lipid metabolic pathway is essential for functional chloroplasts and CO₂ and light responses in *Arabidopsis* guard cells. *Proc. Natl. Acad. Sci. USA* 115: 9038–9043.
- Nishihama, R., Ishizaki, K., Hosaka, M., Matsuda, Y., Kubota, A. and Kohchi, T. (2015) Phytochrome-mediated regulation of cell division and growth during regeneration and sporophyte development in the liverwort *Marchantia polymorpha*. *J. Plant Res.* 128: 407–421.
- Okuda, S., Watanabe, Y., Moriya, Y., Kawano, S., Yamamoto, T., Matsumoto, M., et al. (2017) jPOSTrepo: an international standard data repository for proteomes. *Nucleic Acids Res.* 45: D1107–D1111.
- Okumura, M., Inoue, S., Kuwata, K. and Kinoshita, T. (2016) Photosynthesis activates plasma membrane H⁺-ATPase via sugar accumulation. *Plant Physiol.* 171: 580–589.
- Okumura, M., Inoue, S., Takahashi, K., Ishizaki, K., Kohchi, T. and Kinoshita, T. (2012) Characterization of the plasma membrane H⁺-ATPase in the liverwort *Marchantia polymorpha*. *Plant Physiol.* 159: 826–834.
- Olsen, J.V., de Godoy, L.M.F., Li, G., Macek, B., Mortensen, P., Pesch, R., et al. (2005) Parts per million mass accuracy on an orbitrap mass spectrometer via lock mass injection into a C-trap. *Mol. Cell. Proteomics* 4: 2010–2021.
- Periappuram, C., Steinhauer, L., Barton, D.L., Taylor, D.C., Chatson, B. and Zou, J. (2000) The plastidic phosphoglucosyltransferase from *Arabidopsis*. A reversible enzyme reaction with an important role in metabolic control. *Plant Physiol.* 122: 1193–1200.
- Petrillo, E., Herz, M.A.G., Fuchs, A., Reifer, D., Fuller, J., Yanovsky, M.J., et al. (2014) A chloroplast retrograde signal regulates nuclear alternative splicing. *Science* 344: 427–430.
- Porceddu, A., Stals, H., Reichheld, J.-P., Segers, G., De Veylder, L., de Pinho Barrôco, R., et al. (2001) A plant-specific cyclin-dependent kinase is involved in the control of G₂/M progression in plants. *J. Biol. Chem.* 276: 36354–36360.
- Puttick, M.N., Morris, J.L., Williams, T.A., Cox, C.J., Edwards, D., Kenrick, P., et al. (2018) The interrelationships of land plants and the nature of the ancestral embryophyte. *Curr. Biol.* 28: 733–745.
- Qiu, Y.-L., Li, L., Wang, B., Chen, Z., Knoop, V., Groth-Malonek, M., et al. (2006) The deepest divergences in land plants inferred from phylogenomic evidence. *Proc. Natl. Acad. Sci. USA* 103: 15511–15516.
- Ramel, F., Birtic, S., Ginies, C., Soubigou-Taconnat, L., Triantaphylides, C. and Havaux, M. (2012) Carotenoid oxidation products are stress signals that mediate gene responses to singlet oxygen in plants. *Proc. Natl. Acad. Sci. USA* 109: 5535–5540.
- Rappsilber, J., Mann, M. and Ishihama, Y. (2007) Protocol for micro-purification, enrichment, pre-fractionation and storage of peptides for proteomics using StageTips. *Nat. Protoc.* 2: 1896–1906.
- Schmitz, J., Schöttler, M., Krueger, S., Geimer, S., Schneider, A., Kleine, T., et al. (2012) Defects in leaf carbohydrate metabolism compromise acclimation to high light and lead to a high chlorophyll fluorescence phenotype in *Arabidopsis thaliana*. *BMC Plant Biol.* 12: 8.
- Schneider, A., Häusler, R.E., Kolukisaoglu, Ü., Kunze, R., Van der Graaff, E., Schwacke, R., et al. (2002) An *Arabidopsis thaliana* knock-out mutant of the chloroplast triose phosphate/phosphate translocator is severely compromised only when starch synthesis, but not starch mobilisation is abolished. *Plant J.* 32: 685–699.
- Schroeder, M.J., Shabanowitz, J., Schwartz, J.C., Hunt, D.F. and Coon, J.J. (2004) A neutral loss activation method for improved phosphopeptide sequence analysis by quadrupole ion trap mass spectrometry. *Anal. Chem.* 76: 3590–3598.
- Schultz, J., Milpetz, F., Bork, P. and Ponting, C.P. (1998) SMART, a simple modular architecture research tool: identification of signaling domains. *Proc. Natl. Acad. Sci. USA* 95: 5857–5864.
- Shahzad, Z., Canut, M., Tournaire-Roux, C., Martinière, A., Boursiac, Y., Loudet, O., et al. (2016) A potassium-dependent oxygen sensing pathway regulates plant root hydraulics. *Cell* 167: 87–98.
- Signora, L., Galtier, N., Skot, L., Lucas, H. and Foyer, C.H. (1998) Over-expression of sucrose phosphate synthase in *Arabidopsis thaliana* results in increased foliar sucrose/starch ratios and favours decreased foliar carbohydrate accumulation in plants after prolonged growth with CO₂ enrichment. *J. Exp. Bot.* 49: 669–680.
- Soriano, G., Del-Castillo-Alonso, M.Á., Monforte, L., Tomás-Las-Heras, R., Martínez-Abaigar, J. and Núñez-Olivera, E. (2019) Photosynthetically-active radiation, UV-A and UV-B, causes both common and specific damage and photoprotective responses in the model liverwort *Marchantia polymorpha* subsp. *ruderalis*. *Photochem. Photobiol. Sci.* 18: 400–412.
- Stecker, K.E., Minkoff, B.B. and Sussman, M.R. (2014) Phosphoproteomic analyses reveal early signaling events in the osmotic stress response. *Plant Physiol.* 165: 1171–1187.
- Stitt, M., Gerhardt, R., Kürzel, B. and Heldt, H.W. (1983) A role for fructose 2,6-bisphosphate in the regulation of sucrose synthesis in spinach leaves. *Plant Physiol.* 72: 1139–1141.
- Stitt, M. and Heldt, H.W. (1984) Control of photosynthetic sucrose synthesis by fructose 2,6-bisphosphate. *Plant Physiol.* 79: 599–608.
- Streb, S. and Zeeman, S. (2012) Starch metabolism in *Arabidopsis*. *Arabidopsis Book* 10: e0160.
- Suetsugu, N., Takami, T., Ebisu, Y., Watanabe, H., Iiboshi, C., Doi, M., et al. (2014) Guard cell chloroplasts are essential for blue light-dependent stomatal opening in *Arabidopsis*. *PLoS One* 9: e0108374.
- Sugano, S.S. and Nishihama, R. (2018) CRISPR/Cas9-based genome editing of transcription factor genes in *Marchantia polymorpha*. *Methods Mol. Biol.* 1830: 109–126.
- Sugano, S.S., Nishihama, R., Shirakawa, M., Takagi, J., Matsuda, Y., Ishida, S., et al. (2018) Efficient CRISPR/Cas9-based genome editing and its application to conditional genetic analysis in *Marchantia polymorpha*. *PLoS One* 13: e0205117.
- Sugiyama, N., Masuda, T., Shinoda, K., Nakamura, A., Tomita, M. and Ishihama, Y. (2007) Phosphopeptide enrichment by aliphatic hydroxy acid-modified metal oxide chromatography for nano-LC-MS/MS in proteomics applications. *Mol. Cell. Proteomics* 6: 1103–1109.
- Tyanova, S., Temu, T. and Cox, J. (2016a) The MaxQuant computational platform for mass spectrometry-based shotgun proteomics. *Nat. Protoc.* 11: 2301–2319.
- Tyanova, S., Temu, T., Sinitcyn, P., Carlson, A., Hein, M.Y., Geiger, T., et al. (2016b) The Perseus computational platform for comprehensive analysis of (prote)omics data. *Nat. Methods* 13: 731–740.
- Van Leene, J., Han, C., Gadeyne, A., Eeckhout, D., Matthijs, C., Cannoot, B., et al. (2019) Capturing the phosphorylation and protein interaction landscape of the plant TOR kinase. *Nat. Plants* 5: 316–327.
- Wiśniewski, J.R., Zougman, A., Nagaraj, N. and Mann, M. (2009) Universal sample preparation method for proteome analysis. *Nat. Methods* 6: 359–362.
- Xiong, Y., McCormack, M., Li, L., Hall, Q., Xiang, C. and Sheen, J. (2013) Glucose–TOR signalling reprograms the transcriptome and activates meristems. *Nature* 496: 181–186.